



Research articles

Effect of a high magnetic field on hard magnetic multilayered Fe-Pt alloys

Lin Zhang^{a,*}, Ke Han^{b,*}, Xiaorong Zhang^a, Engang Wang^{a,*}, Jun Lu^b, Robert Goddard^b^a Key Laboratory of Electromagnetic Processing of Materials (Ministry of Education), Northeastern University, Shenyang 110819, Liaoning, China^b National High Magnetic Field Laboratory, Florida State University, Tallahassee 32310, FL, USA

ARTICLE INFO

Keywords:

Fe-Pt
Multilayer
Annealing
High magnetic field (HMF)
Magnetic properties

ABSTRACT

Fe-50 vol%Pt multilayers that were prepared by accumulative roll-bonding were annealed in vacuum for 2 h at various temperatures between 723 K and 823 K. Some samples were annealed without any high magnetic field (HMF). Others were subjected HMF up to 31.2 T, applied in either in-plane or out-of-plane directions. The annealing partially transformed the original multilayered structure into a polycrystalline hard-magnetic FePt magnetic phase with ordered L1₀ structure. Textured FePt/Fe nanocomposite foils were formed under HMF. Magnetic anisotropic behavior was observed in the annealed FePt/Fe composite because of the textured nanostructure. HMF annealing decreased grain size and increased the (0 0 1) texture along the HMF direction. In the sample annealed with out-of-plane HMF, both coercivity and maximum energy product were enhanced because of higher (0 0 1) out-of-plane texture and finer nanoscaled grain sizes compared to other samples. An in-plane HMF appeared to strongly inhibit phase transformation. This inhibition likely resulted from a change in Gibbs free energy and the diffusion inhibition caused by HMF.

1. Introduction

Fe-Pt nanostructured alloys are known to have both high magnetization and high uniaxial magnetocrystalline anisotropy [1]. These alloys have drawn extensive attention and are candidates for use as exchange-spring magnets, a type of permanent magnet with a high energy product. These magnets consist of exchange-coupled hard and soft magnetic phases [2]. There are three intermetallics (Fe₃Pt, FePt and FePt₃) in Fe-Pt alloys. When the Fe and Pt atoms are randomly arranged, these intermetallics have a face-centered cubic (fcc) structure at room temperature [3]. As an ordered alloy, FePt has face-centered tetragonal (fct) L1₀ structure, which consists of alternating planes of Fe atoms and Pt atoms stacked along the [0 0 1] direction. It is this structure that gives rise to high magnetocrystalline anisotropy and high magnetic coercivity [1]. Fe₃Pt may crystallize in an ordered cubic L1₂ structure in which the Fe atoms occupy the face centers and the Pt atoms the cube corners. In Fe-rich Fe-Pt alloys, hard magnetic FePt phase and soft magnetic Fe₃Pt/α-Fe phase coexist, producing an exchange-spring magnet [3,4].

Films or foils of Fe-Pt have previously been prepared by a number of techniques including molecular beam epitaxy (MBE) [5], cosputtering [6], sputtering of Fe/Pt multilayers [2], and accumulative roll bonding of Fe/Pt multilayers (ARB) [7]. Annealing of the precursor of magnetic alloys under high magnetic field can increase magnetic moment,

anisotropy and maximum energy product (BH)_{max} [8–16]. For Fe-Pt films, annealing under a magnetic field enhance the coercivity, refine the grain [17], and augment the texture [4].

Researchers have made multilayer Fe/Pt by means of the accumulated roll bonding (ARB) process. They have studied the formation of the high anisotropy L1₀ FePt phase by means of controlled diffusion and ordering [3]. Other researchers have enhanced crystallographic texture and magnetic properties by annealing the ARB Fe/Pt multilayer under a 19 T magnetic field [4]. Their (BH)_{max} values, however, are still below theoretical value and could be improved. Further improvement in texture could be gained by using a higher magnetic field (HMF). The aim of this work is to study in detail the effect of HMF on Fe-Pt nanostructured alloys. Using TEM, we observed certain structural characteristics in cross-section view, revealing more information about phase transformation that had been previously reported based on plan-view TEM results [3].

In the present work, ARB was used to synthesize Fe-50 vol% multilayers. Magnetic annealing was performed under HMF of 31.2 T. We studied the ways in which the microstructure and magnetic properties were affected by the annealing temperature, along with the strength and direction of the HMF.

* Corresponding authors.

E-mail addresses: zhanglin@epm.neu.edu.cn (L. Zhang), han@magnet.fsu.edu (K. Han), egwang@mail.neu.edu.cn (E. Wang).<https://doi.org/10.1016/j.jmmm.2019.165533>

Received 6 May 2019; Received in revised form 26 June 2019; Accepted 5 July 2019

Available online 06 July 2019

0304-8853/© 2019 Elsevier B.V. All rights reserved.

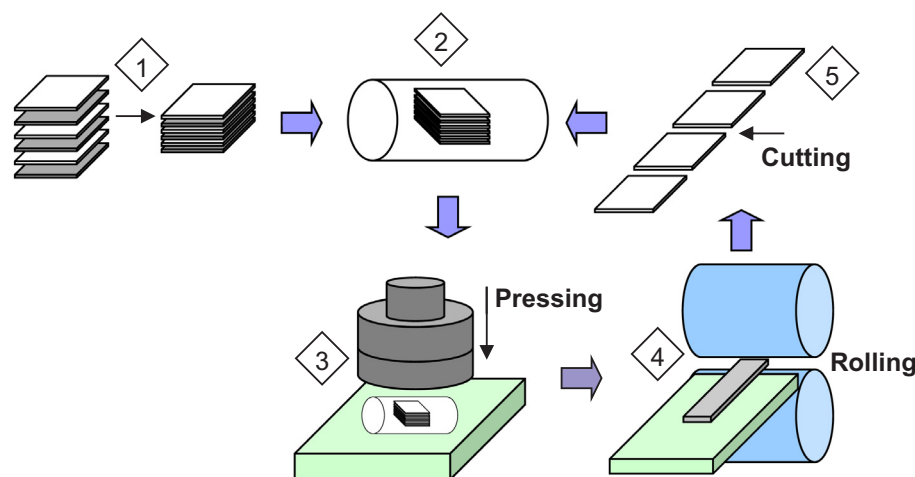


Fig. 1. Accumulative roll bonding process. The Fe content 43.83 at% was estimated from the measured masses. The total thickness of the multilayer is 100 μm . (1) Cutting and stacking of Fe and Pt foils, (2) Insertion of stack into a stainless steel sheath, (3) Pressing of the assembled sheath, (4) Rolling of the pressed sample, (5) sheath removal, cutting and re-assembly of the deformed composite foil.

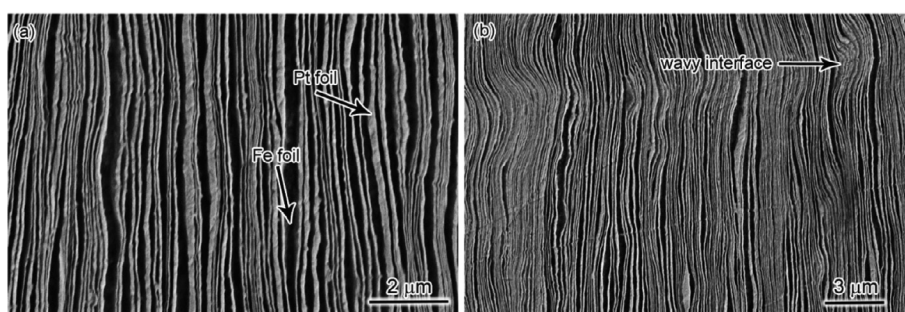


Fig. 2. SEM image of the ARB Fe/Pt multilayer: Fe appears dark and Pt appears grey: (a) After the 5th rolling cycle, the average layer thickness was estimated to be 112 nm; (b) After the 6th rolling cycle, the average layer thickness was estimated to be 42 nm.

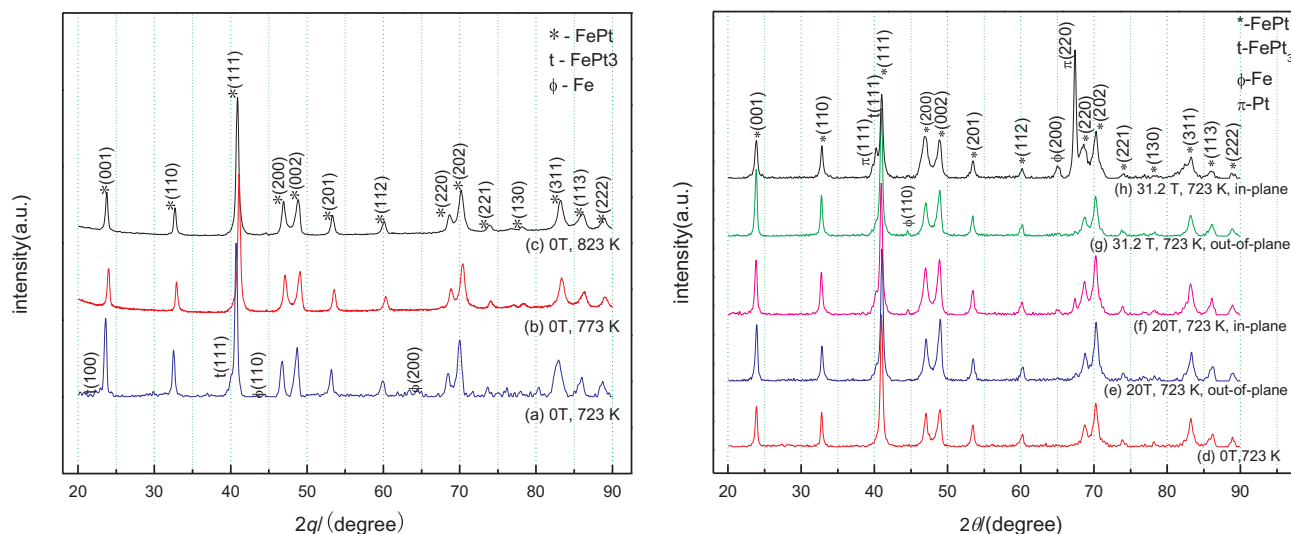


Fig. 3. XRD patterns of annealed Fe-Pt multilayers (a–c) after the 5th rolling cycle, annealed at various temperatures for 2 h, and XRD patterns of annealed Fe-Pt multilayers (d–h) after the 6th rolling cycle, annealed at 723 K for 2 h under different magnetic fields. The corresponding microstructure is shown in Fig. 2a and b. The presence of Pt (1 1 1) is indicated by a sloping “shoulder” on one side of the base of the FePt (1 1 1) peak. The 2θ values of (1 1 1)_{Pt}, (1 1 1)_{FePt₃}, and (1 1 1)_{FePt} are 39.763°, 40.452°, and 41.049°, respectively. (That is to say, the peak at the 2θ value near 40° in Fig. 3h might be a mix of 3 different peaks of Pt, FePt₃, and FePt.) The out-of-plane texture can be indicated by the intensity ratio of (0 0 2) over (2 0 0), which is highest (47%) in an out-of-plane HMF of 31.2 T. In an in-plane HMF of 31.2 T, the intensity of Pt peaks is much higher than that of FePt peaks or Fe peaks (Fig. 3h). This is partly owing to the fact that the atomic number of Pt is much higher than that of Fe. The presence of small FePt₃ and Fe peaks indicates the small amount volume fraction of both phases.

2. Experimental procedure

Fe-Pt magnetic foils were prepared by the ARB of Fe and Pt foils down to the nano scale (43.83 at% Fe), as illustrated in Fig. 1. The starting sample used for accumulative roll bonding consisted of an

alternate stacking of foils of two different materials with individual foil thicknesses on the order of 25 μm . Ten bilayers of Fe and Pt foils [Fe (25 μm)/Pt(25 μm)]₁₀ were first stacked to a total thickness of at least 0.5 mm. The stacked bilayers were placed in a sheath of stainless steel (see schematic in Fig. 1). The ensemble was compressed under pressure

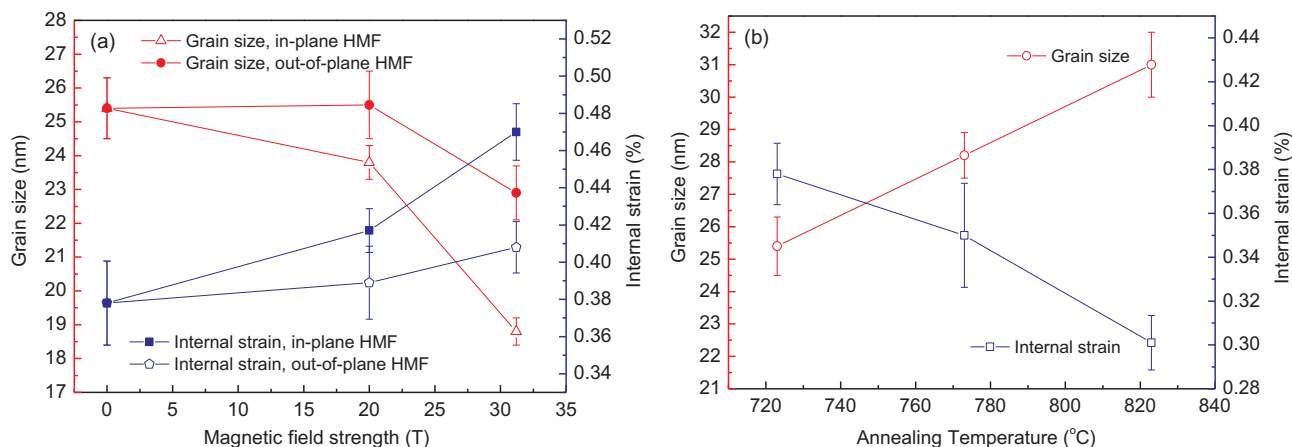


Fig. 4. Grain size and internal strain of Fe-Pt samples as a function of magnetic field strength (a) and annealing temperatures (b). (a) The left vertical axis describes grain sizes for samples annealed at 723 K in either in-plane (hollow triangle) or out-of-plane (solid circle) HMF. The right vertical axis describes internal strains for samples annealed at 723 K in either in-plane (solid square) or out-of-plane (hollow pentagon) HMF. (b) The left vertical axis describes grain sizes for samples annealed at various temperatures (hollow circle). The right vertical axis describes internal strains for samples annealed at various temperatures (hollow square).

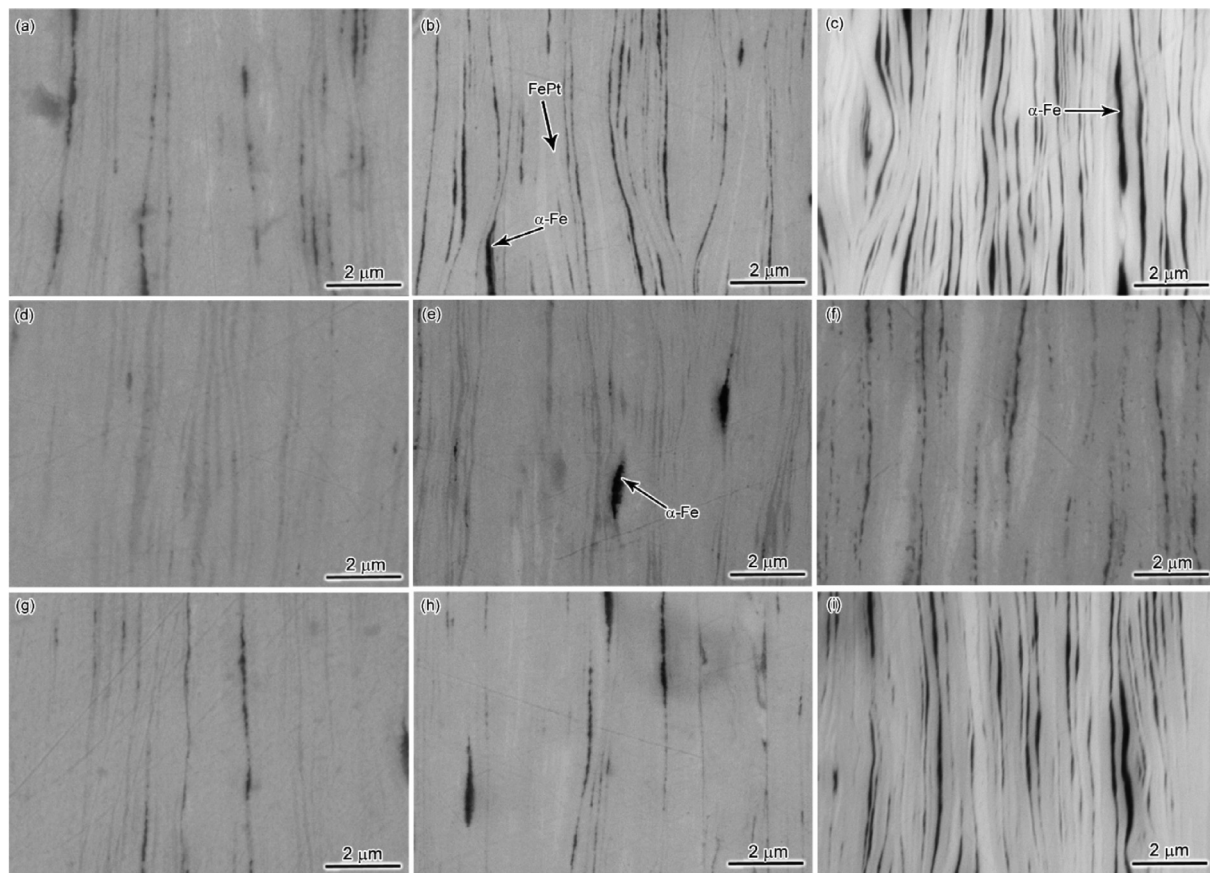


Fig. 5. Cross-sectional SEM images of Fe-Pt after 5th (a-f) and 6th (g-i) rolling cycle and annealing. The grey regions are mainly FePt phase while the dark regions are mainly α -Fe phase according to the EDS results. (a) 0 T, 723 K; (b) 31.2 T out-of-plane, 723 K; (c) 31.2 T in-plane, 723 K; (d) 0 T, 823 K; (e) 31.2 T out-of-plane, 823 K; (f) 31.2 T in-plane, 823 K; (g) 0 T, 723 K; (h) 31.2 T out-of-plane, 723 K; (i) 31.2 T in-plane, 723 K.

of about 5 ton/cm^2 under ambient conditions and then cold-rolled for the desired number of cycles. One cold-rolling cycle included three rolling passes at room temperature for a total thickness reduction ~ 70 – 80% . A cycle included cutting, stacking, inserting into a sheath, and compressing. Each sample subjected to at least one cycle; none underwent less than eight. The final manufactured samples were roughly $100 \mu\text{m}$ thick. Deformation was performed without intermediate annealing in order to avoid formation of any intermetallic

compounds, which might embrittle the material due to the limited plasticity of intermetallic compounds at room temperature.

Several small samples ($\sim 5 \text{ mm} \times 5 \text{ mm}$) were cut from the central part from each as-rolled Fe/Pt foils. These samples were then sealed in a vacuum quartz tube and annealed under zero, 20 T, and 31.2 T in-plane HMF for 2 h at temperatures between 723 and 823 K. During HMF annealing, the HMF was applied in the rolling direction; that is, in-plane field. The magnetic field was reduced to zero when the samples were cooled down

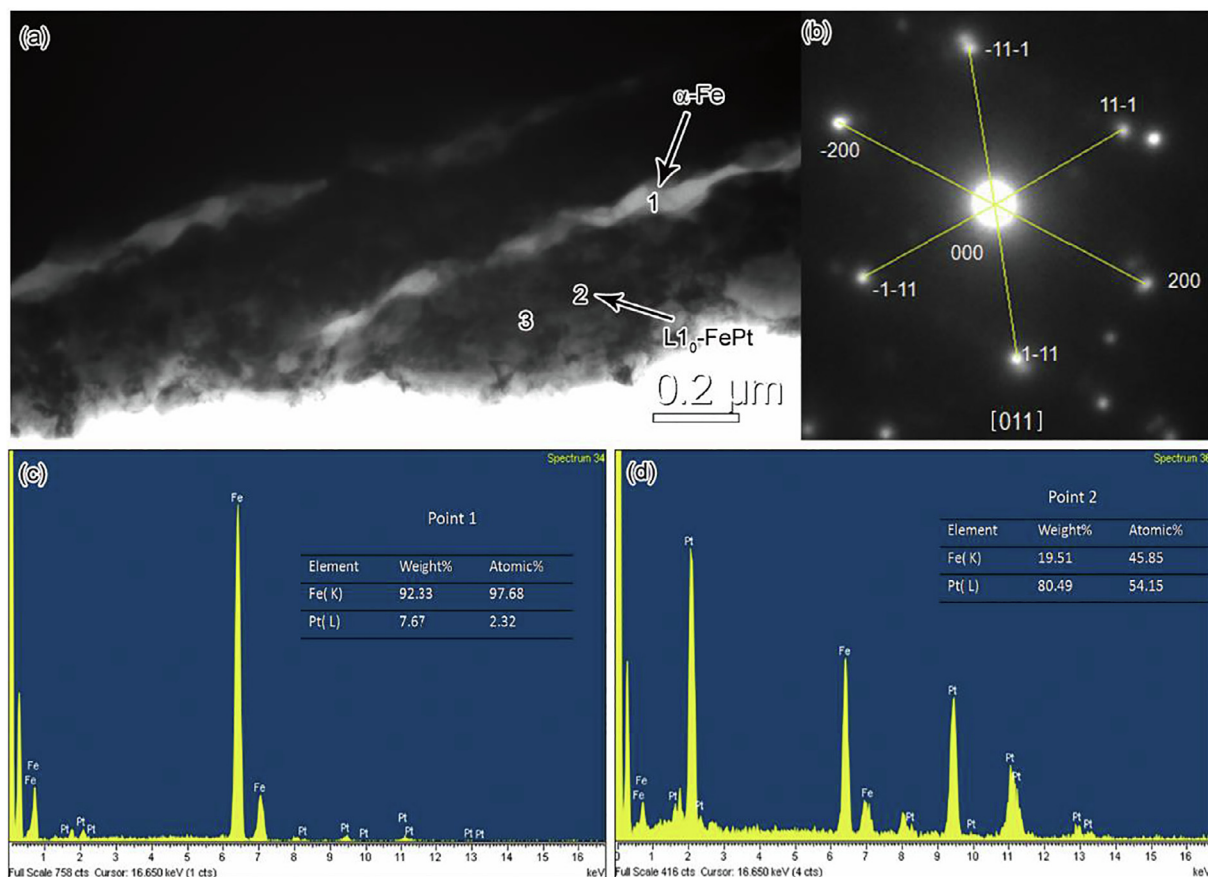


Fig. 6. TEM image and corresponding EDS results from Fe-Pt sample annealed at 723 K for 2 h without magnetic field: (a) parallel white layers were identified by EDS (Fig. 6c) to be α -Fe phase (SEM showing dark contrast in Fig. 5); α -Fe being embedded in dark matrix of $L1_0$ -FePt phase identified by (b) diffraction pattern from location 3 in $[011]$ zone axis. Selected diffraction spots were indexed; (c) EDS results at location 1; (d) EDS results at location 2.

Table 1

Volume fraction of Fe in samples annealed under zero and 31.2 T in different orientations.

	Vol%Fe (0 T)	Error	Vol%Fe (31.2 T, Out of plane)	Error	Vol%Fe (31.2 T, In plane)	Error
5 cycle	1.24	0.38	3.80	1.34	14.68	2.58
6 cycle	0.81	0.29	1.85	0.84	9.56	0.60

below 673 K. To compare the influence of magnetic direction, HMF was also applied in the direction perpendicular to the plane of the Fe-Pt samples; that is out-of-plane field.

Scanning Electron Microscopy (SEM) images were taken in a Zeiss 1540 EsB field-emission scanning electron microscope. Transmission Electron Microscopy (TEM) images were taken with a FEI Tecnai G² 20 transmission electron microscope. X-Ray Diffraction (XRD) measurement was performed with a PANalytical X'pert pro X-ray diffractometer (XRD) using Cu K α radiation. Magnetic properties were measured in a Quantum Design Physical Property Measurement System (PPMS) in fields up to 4 T. The demagnetization factor for out-of-plane curve was chosen as 1 because the specimen was treated as a flat sheet perpendicular to the magnetic field.

3. Results and discussions

3.1. Structure of ARB Fe/Pt multilayers

The morphology of multilayers is strongly dependent on ARB

conditions. SEM images cross-sectioned in the longitudinal direction were used to show the progress of the microstructural refinement of Fe/Pt multilayers as their thickness was gradually reduced (Fig. 2). Fe and Pt layers were neither flat nor perfectly homogeneous in thickness, but they remained continuous throughout the sample. Interfaces between Fe and Pt appeared sharp. Neither amorphization nor intermetallic phases were observed. The average thickness of individual layers was estimated by dividing the total foil thickness by the designated number of layers. A few layers were found to be several times thicker than most. Layer thickness in samples rolled to the 3rd, 4th, 5th, or 6th cycle was 1 μ m, 251 nm, 112 nm, and 42 nm, respectively. In individual layers, wavy or kinked interfaces were observed after each rolling step. We attributed this inhomogeneity to the shear introduced by severe plastic deformation or to insufficient welding in one or more of the re-stacking steps.

3.2. Phases and texture of annealed Fe-Pt multilayer

X-ray diffraction (XRD) was used to identify phases and texture in FePt samples annealed under different conditions (Fig. 3). In all annealed samples, XRD results showed face-centered tetragonal (fct) FePt phase. In these samples, the $(002)_{\text{FePt}}$ peak was not only higher than the $(200)_{\text{FePt}}$ peak, but also the ratio of $(002)_{\text{FePt}}$ over $(200)_{\text{FePt}}$ was 20–76% higher than the standard ratio found in powder samples. Thus, our samples showed c-axis out-of-plane texture, which could offer highly desirable anisotropic magnetic properties.

In samples annealed without HMF at various temperatures, increasing the annealing temperature led to a higher volume fraction of $L1_0$ FePt phase, accompanied by a lower volume fraction of Fe and

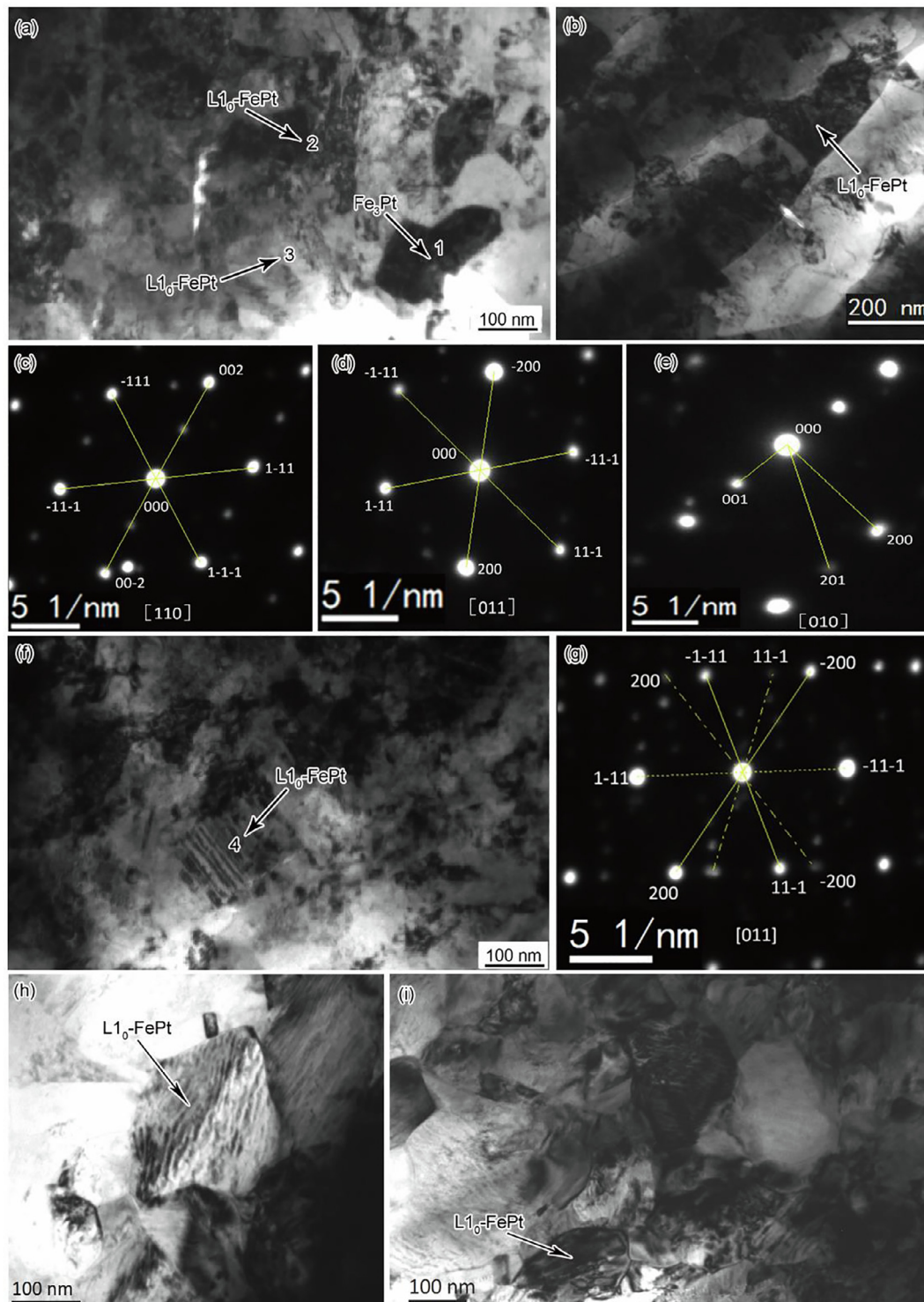


Fig. 7. TEM results of annealed Fe-Pt samples subjected to 6th cycle of rolling (a, b, f) annealed without magnetic field; (c) diffraction pattern at location 1 identified as Fe_3Pt phase; (d-e, g) diffraction patterns at locations 2, 3 and 4 showing $\text{L1}_0\text{-FePt}$ phase; (h) TEM image of a sample annealed at 723 K with a 20 T out-of-plane magnetic field; (i) TEM image of a sample annealed at 723 K with a 31.2 T out-of-plane magnetic field;

FePt_3 phases. In samples subjected to five complete rolling cycles and annealed at 723 K, a small amount of Fe and FePt_3 phases remained because of incomplete phase transformation (see Fig. 3a). In the samples annealed at 773 K and 823 K, Fe and FePt_3 had disappeared, indicating that the phase transformation was complete. The same was true of samples subjected to six rolling cycles and annealed at 723 K without HMF. Completion of phase transformation usually requires higher annealing temperatures, but in the samples subjected to six

rolling cycles, phase transformation could be completed at lower temperatures because the additional rolling cycle decreased the thickness of each individual layer. A thickness that is generally equivalent to half of the diffusion distance is necessary for phase transformation to be completed. In the sample annealed at 723 K, the intensity ratio of (002) over (200) was higher than in samples annealed at higher temperatures, indicating a higher out-of-plane (001) texture, which may indicate stronger anisotropic magnetic properties.

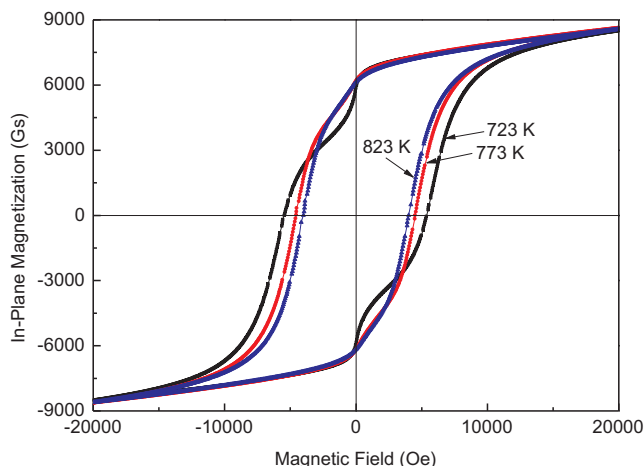


Fig. 8. In-plane hysteresis curves of Fe-Pt foils (5th rolling cycles) annealed at different temperatures without HMF. After processing the magnetic properties of the sample were measured in a PPMS with magnetic field up to 40 kOe. Sample annealed at 723 K has the least phase transformation. A shoulder in the hysteresis curve indicates that the relatively poor exchange-coupling between the phases.

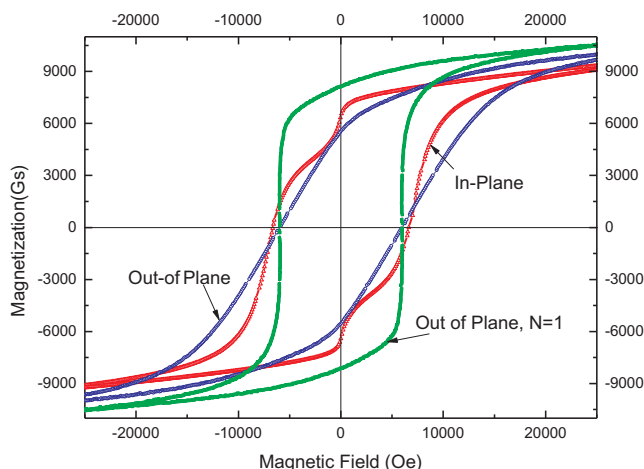


Fig. 9. Hysteresis curves of Fe-Pt foils (6th rolling cycle) annealed at 723 K with a 31.2 T out-of-plane HMF: curves marked by “in-plane” and “out-of-plane” indicate the direction of the magnetic field applied by the magnet in a PPMS during hysteresis curve measurements.

Application of HMF during annealing had a marked effect on XRD peak ratios. Comparison of X-ray data from samples annealed at 723 K for 2 h under different levels and orientations of HMF indicates that out-of-plane FePt (0 0 1)_{FePt} texture increased with increasing out-of-plane-HMF (Fig. 3d–h). Annealed foils subjected to the highest out-of-plane HMF in our study (31.2 T) showed the highest out-of-plane (0 0 1)_{FePt} texture (Fig. 3g). In samples subjected to in-plane HMF at the same level, out-of-plane (0 0 1)_{FePt} texture was reduced, as indicated by the reduction of intensity of the (0 0 2)_{FePt} peak by 9% below that of the (2 0 0)_{FePt} peak (Fig. 3h). Because (2 0 0)_{FePt} is perpendicular to (0 0 2)_{FePt}, which is intended to parallel to HMF during the annealing, and HMF was applied in-plane, the decrease of intensity ratio of (0 0 2) over (2 0 0) may indicate an enhancement of in-plane (0 0 1)_{FePt} texture.

XRD results from samples annealed under an in-plane HMF demonstrated the presence of Fe, Pt, and FePt_3 . The XRD intensities of Fe, Pt, and FePt_3 were greater in these samples than in those annealed under out-of-plane HMF, indicating that field orientation affects the kinetics of phase transformation. Compared to samples annealed without any HMF or with out-of-plane HMF, those annealed under in-

plane HMF showed slower phase transformation.

By measuring the full-width-at-half-maximum (FWHM) of the (1 1 1) peak and applying Williamson-Hall plots, we estimated both average grain size and internal strain of FePt (Fig. 4). In the specimens annealed at 723 K under HMF of 0 T, 20 T, and 30.1 T, the averages of grain size were 25.4, 24.1, and 18.8 nm, respectively, and the internal strain ranged from 0.38% up to 0.47%. In another words, as the strength of HMF increased, internal strain increased, and grain size decreased. These trends were less pronounced in samples annealed under an out-of-plane field.

Without any HMF, average grain sizes ranged from 25.4 nm at 723 K to 31 nm at 823 K. Internal strain ranged from 0.3% to 0.38%. In other words, as annealing temperature increased without HMF, grain size increased and internal strain decreased.

3.3. Annealed microstructure of ARB Fe-Pt foil

Cross-sectional SEM images of samples annealed under different conditions showed that the multilayered nanostructure of annealed samples remained similar to that of as-rolled Fe-Pt foils (Fig. 5). Cross-section TEM images taken from samples rolled for five cycles and annealed at 723 K revealed layers of α -Fe with a thickness from 50 to 100 nm (Fig. 6 a and c). Regardless of annealing temperatures, samples emerged with a significantly reduced volume fraction of Fe phase compared with as-rolled multilayers (Fig. 2). Increased annealing temperature resulted in increased solid-state transformation. For example, in samples annealed at 823 K, more fct-FePt and less Fe was found than in similar samples annealed at 723 K (see Fig. 5a–f). This is consistent with XRD results that showed more Fe and Pt transformed to FePt at higher annealing temperatures.

After annealing at 723 K for 2 h, Fe-Pt foils that had been rolled for six cycles had fewer Fe layers visible than samples rolled to five cycles (cf. Fig. 5a–f for fifth rolling cycle and Fig. 5g–i for sixth rolling cycle). This indicates that an ARB multilayer with thinner bilayer thickness is more likely to undergo complete phase transformation (see Table 1).

Both SEM images and XRD results showed that phase transformation ($\text{Fe} + \text{Pt} \rightarrow \text{fct-FePt}$) is affected by both the level and the orientation of HMF during annealing (Table 1, Figs. 3 and 5). For example, the highest volume fraction of Fe layers was found in samples annealed in an in-plane HMF of 31.2 T, and the lowest volume fraction of Fe was found in samples annealed without any HMF at all. An out-of-plane HMF also inhibited phase transformation, but at a modest level.

TEM results showed that the interface between α -Fe and matrix appeared to be wavy, resulting probably from rolling. EDS results showed that the Fe content in the matrix was $46 \pm 3.5\%$.

TEM cross-section images showed that most regions within the annealed Fe-Pt samples had equiaxial grains. Most of these were identified as L1_0 -FePt by selected area diffraction patterns (SADP) but some were Fe_3Pt phase (Fig. 7a, c). The dimension of the L1_0 -FePt grains varied from tens to hundreds of nanometers. This dimension is similar to that reported in plan-view images [7], indicating that the original multilayered structure had no significant effect on 3-dimensional growth of L1_0 -FePt grains. Cross-section TEM images appeared to show larger grain sizes than those estimated from XRD results. There are two reasons for this: 1) Twin boundaries may form because of internal strain energy stored during the cold-ARB process. XRD results showed all grain boundaries, including twin boundaries, while TEM results may have missed some twin boundaries if samples were not tilted properly (Fig. 7f & g). 2) Large strain resulting from deformation may result in a contrast in the TEM images that obscures the grain boundary of small grains.

Most of our TEM images confirmed that application of HMF inhibited grain growth in L1_0 -FePt so that the grain size in samples annealed under 31.2 T appeared smaller than that of samples annealed under 20 T (Fig. 7h & i).

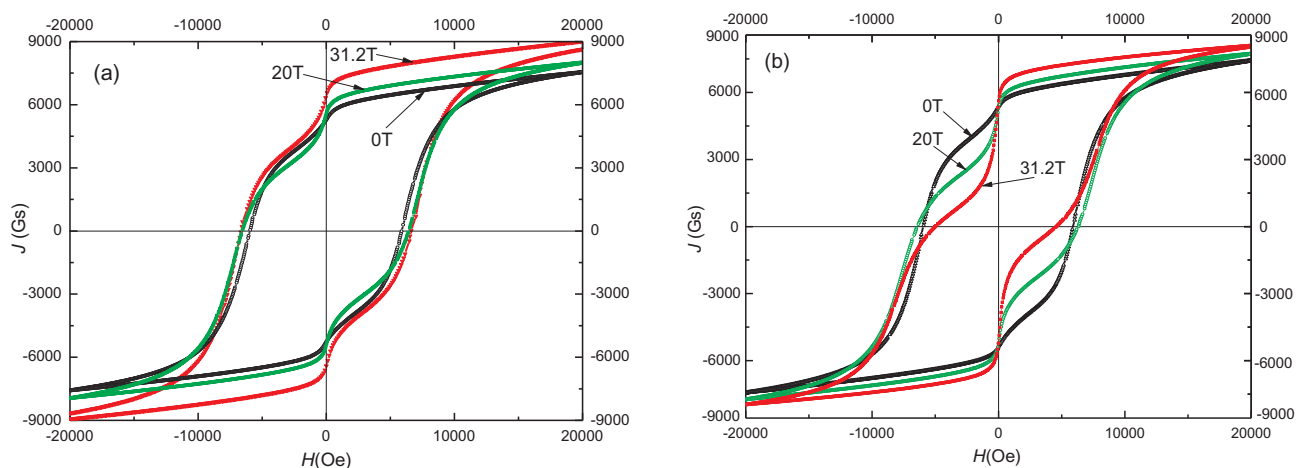


Fig. 10. Room temperature in-plane hysteresis curves of Fe-Pt foils (6th rolling cycles) annealed at 723 K with different fields. The hysteresis curves are generated with in-plane field in PPMS. (a) out-of-plane HMF; (b) in-plane magnetic field. H_{ci} values are 5.9 kOe, 6.5 kOe, and 6.6 kOe for samples annealed without HMF and with out-of-plane 20 and 31.2 T HMF, respectively. All the hysteresis loops showed uncoupled soft magnetic phases, indicated by shoulders. The shoulder showed at lower magnetization values in samples annealed with an in-plane field. The shoulder location affected the estimated $(BH)_{max}$.

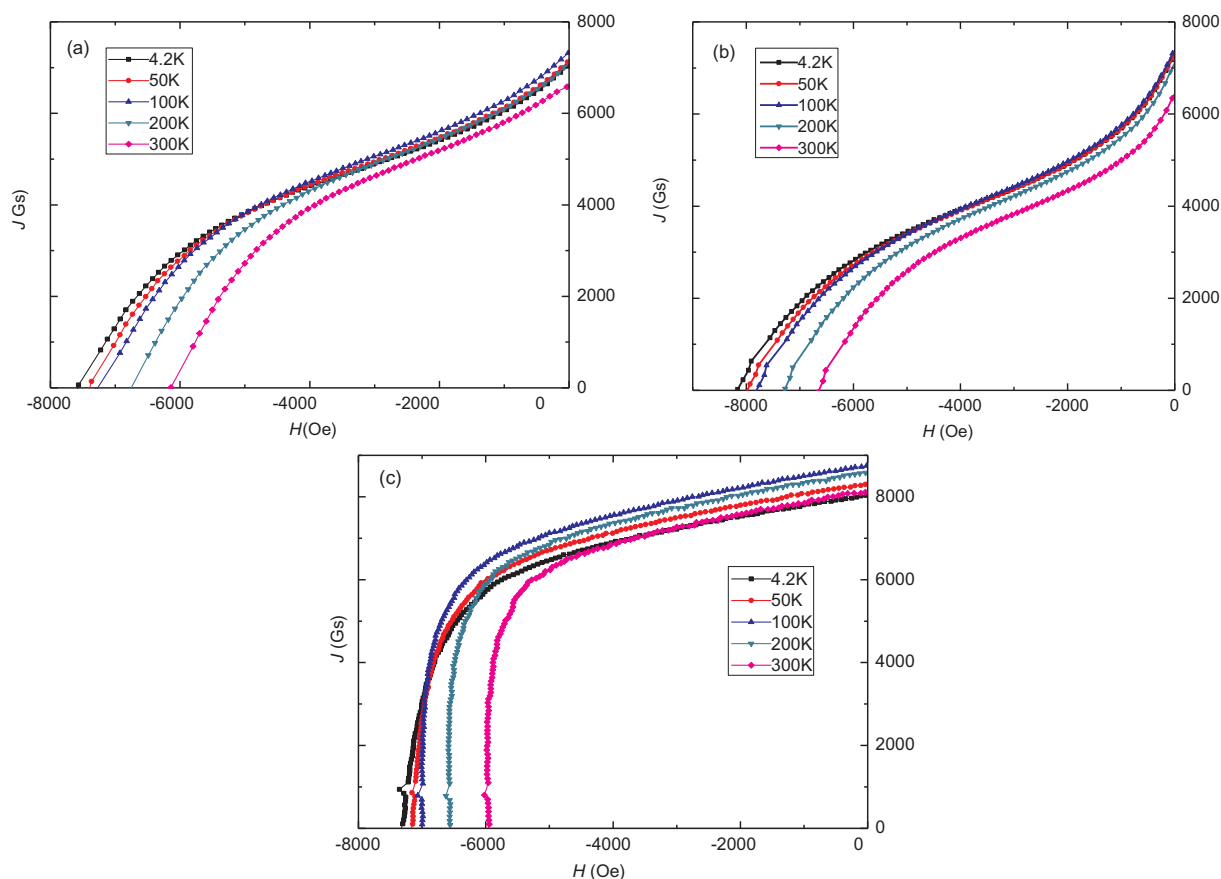


Fig. 11. Demagnetizing curves measured at different temperatures for Fe-Pt foils annealed at 723 K after 6th rolling cycles (a) 0 T, measured by in-plane field; (b) Annealed with 31.2 T out-of-plane field, measured by in-plane field; (c) Annealed with 31.2 T out-of-plane field, measured by out-of-plane field, demagnetizing factor $N = 1$.

3.4. Magnetic properties

Three samples rolled to five cycles and annealed at various temperatures without HMF were measured at 300 K. The resulting magnetization hysteresis curves showed that annealing temperature itself had almost no effect on remanence (B_r) (Fig. 8). Magnetic coercivity (H_{ic}) varied around 5 kOe and decreased as annealing temperatures increased. The highest H_{ic} was found in samples annealed at 723 K

because these samples had the smallest grains. Smaller grains correspond to larger grain boundary area within a given unit area. Domain walls are pinned by those grain boundaries.

Magnetic anisotropy was shown in Fe-Pt foils rolled to 6 cycles and annealed at 723 K under an out-of-plane HMF of 31.2 T. The values of out-of-plane and in-plane H_{ic} were about 6.1 kOe and 6.6 kOe, respectively. This magnetization anisotropy is attributable to [0 0 1] texture in $L1_0$ FePt phase, as reported in our XRD results (Fig. 3).

Table 2

Coercivity, remanence and energy product in the hysteresis curves of Fe-Pt foils annealed at 723 K after 6th rolling cycles. Error bars for coercivity, remanence, and energy product are 0.5%, 0.5%, and 1%, respectively.

Specimens	Measured temperature/K	Coercivity (H_{ic})/kOe	Remanence (Br)/kGs	Energy product, $(BH)_{max}/\text{kJ/m}^3$
0 T, measured by in-plane field	4.2	7.56	7.03	54.28
	50	7.40	7.13	55.29
	100	7.26	7.33	57.52
	200	6.75	7.08	55
Annealed with 31.2 T out-of-plane field, measured by in-plane field	300	6.14	6.58	50.92
	4.2	8.15	7.24	46.61
	50	7.98	7.25	46.49
	100	7.78	7.37	47.41
Annealed with 31.2 T out-of-plane field, measured by out-of-plane field	200	7.27	7.07	44.04
	300	6.62	6.39	37.9
	4.2	7.30	8.04	101.31
	50	7.14	8.32	107.84
Annealed with 31.2 T out-of-plane field, measured by out-of-plane field	100	7.01	8.76	118.58
	200	6.56	8.59	113.9
	300	5.95	8.12	76.96

Exchange coupling between the soft magnetic phase and the hard magnetic $L1_0$ phase was not complete, as shown by a shoulder in the in-plane hysteresis curve (Fig. 9). This incomplete coupling occurred also in materials annealed without the magnetic field. Similar curves have been recorded by previous researchers [1,18–20]. In our study, we found that the soft phase consisted of thin layers of α -Fe phase and small quantities of Fe_3Pt or FePt_3 embedded in $L1_0$ FePt, as identified by both TEM and XRD.

Magnetic properties were governed by the orientation and strength of the HMF we applied during the annealing process (Fig. 10). For example, increasing HMF enhanced H_{ci} . Applying 20 T and 31.2 T HMF perpendicular to the foil surface increased H_{ci} by 10 and 12%, respectively (Fig. 10a). Under both in-plane and out-of-plane HMF, remanence and saturation magnetization increased with increasing magnetic field strength.

As out-of-plane HMF strength increased, energy product increased, but as in-plane HMF strength increased, energy product decreased. The sample annealed under an out-of-plane HMF of 31.2 T showed the highest energy product, but the sample annealed under an in-plane HMF of the same strength had the lowest energy product. The reduction in energy products can be explained by incomplete phase transformation, which allowed more α -Fe phase to remain in samples annealed

under an in-plane HMF.

Demagnetizing curves of samples annealed at 723 K showed that out-of-plane HMF increased in-plane H_{ic} at all measured temperatures (Fig. 11 & Table 2). Annealing a sample under an out-of-plane HMF of 31.2 T, for example, enhanced its in-plane H_{ic} from ~ 6.14 kOe to ~ 6.62 kOe at 300 K, and from 7.56 kOe to 8.15 kOe at 4.2 K. Out-of-plane H_{ic} , however, was reduced by only 3% in a sample annealed under an out-of-plane HMF of the same strength. Because of enhanced out-of-plane texture, out-of-plane HMF of 31.2 T significantly enhanced out-of-plane Br and $(BH)_{max}$ at all measured temperatures (Table 2).

3.5. The effect of high magnetic field on Fe/Pt transformation

The salient feature in current work is that HMF annealing played an important role by enhancing the texture and inhibiting the coarsening of $L1_0$ grains in phase transformation from ARB Fe/Pt multilayers to hard magnetic $L1_0$ phase. HMF may have three possible ways to affect the kinetics for the formation of ordered $L1_0$ FePt.

First, HMF affected nucleation rates by altering the driving force for phase transformation. Nucleation rate can be expressed as [21]:

$$N = \omega C_0 \exp\left(-\frac{\Delta G_m}{RT}\right) \exp\left(-\frac{\Delta G^*}{RT}\right) \quad (1)$$

where C_0 is the number of atoms per unit volume in the phase as a constant. ω is a factor that includes the vibration frequency of the atoms and the area of the critical nucleus. The activation energy for atomic migration is ΔG_m per atom. If both ω and ΔG_m are assumed to be constants, the nucleation rate is controlled by the nucleation barrier ΔG^* :

$$\Delta G^* = -\frac{C\gamma^3}{(\Delta G_V - \Delta G_S)^2} \quad (2)$$

where C is a constant. γ is the interfacial energy. ΔG_S is the misfit strain energy per unit volume. The main factor affecting ΔG^* is the driving force for transformation ΔG_V , which can be affected by HMF.

The velocity of interface growth is expressed as:

$$v = B_0 \exp\left(-\frac{\Delta G_m}{RT}\right) \left[1 - \exp\left(-\frac{\Delta G_V}{RT}\right)\right] \quad (3)$$

B_0 is the ability of the existing transformed phase to accept new atoms and can be assumed constant. Eq.3 indicates that v is also controlled mainly by driving force ΔG_V . ΔG_V is provided by the mole free energy difference between parent and product phases. The parent phases are Fe and Pt, and the product phase is mainly $L1_0$ FePt.

ΔG_V is composed of the chemical contribution $\Delta G_{V,chem}$ and of the magnetic contribution $\Delta G_{V,mag}$ as shown by [22]:

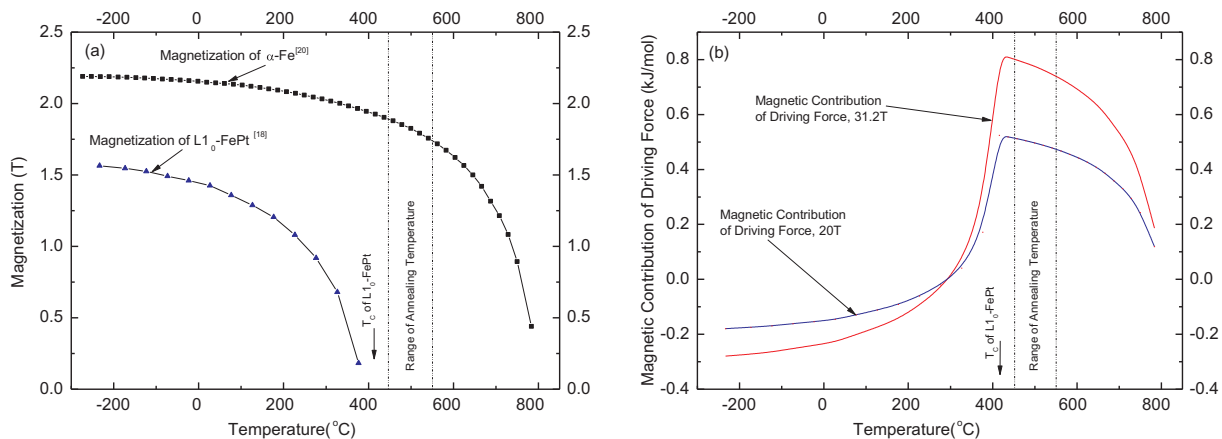


Fig. 12. Magnetization of Fe and FePt (a), and the Magnetic contribution of driving force in 20 T and 31.2 T magnetic field (b). The Magnetization of α -Fe and $L1_0$ -FePt in Fig. 12a is from Ref. [24] and Ref. [26] respectively.

$$\Delta G_V = \Delta G_{V,chem} + \Delta G_{V,Mag} \quad (4)$$

For the reaction, parent phases are α -Fe and Pt, which are ferromagnetic phase and paramagnetic phase in the temperature range used. Oriented Fe_3Pt and FePt_3 phases are the reaction products. The Fe_3Pt and FePt_3 phase have the ordered, cubic L1_2 structure and exhibit ferromagnetic behavior at room temperature, but these phases show paramagnetic behavior in the annealing temperature range [23]. Therefore only the Gibbs free energy of FePt and Fe can be lowered by HMF during transformation. $\Delta G_{V,Mag}$ is the change of Gibbs free energy due to the application of a magnetic field and can be expressed as following equation:

$$\Delta G_{V,Mag} = -\frac{1}{\mu_0} \int_0^B \left(\frac{m^{\text{FePt}}}{\rho^{\text{FePt}}} M^{\text{FePt}} - \frac{m^{\text{Fe}}}{\rho^{\text{Fe}}} M^{\text{Fe}} \right) dB \quad (5)$$

where M^{FePt} and M^{Fe} are the magnetizations of L1_0 -FePt phase and α -Fe phase respectively, and B is the magnetic flux density. m^{FePt} , m^{Fe} , ρ^{FePt} , and ρ^{Fe} are the molar mass of FePt and Fe, the density of FePt and Fe respectively. μ_0 is the magnetic permeability of vacuum. The Curie temperature of bulk L1_0 FePt is $\sim 477^\circ\text{C}$ (Fig. 12a), whereas the nanocrystal FePt has a Curie temperature much lower than 477°C [24]. The annealing temperature in this experiment might be all above the Curie temperature of L1_0 FePt, and the magnetization of FePt is very low in this temperature range. Our calculation using equation (5) indicates that the value of $\Delta G_{V,Mag}$ is high at the annealing temperature, and the value is much higher in a 31.2 T field than that in a 20 T field (Fig. 12b). The positive value of $\Delta G_{V,Mag}$ means that the mole free energy difference between parent and product phases ΔG_V is decreased. Therefore, the driving force is decreased and the applied magnetic field increases the nucleation barrier according to Eq.2, and thus decreases the nucleation rate (see Eq. (1)). The velocity of interface growth is also decreased (see Eq. (3)). The chemical driving force for FePt ordering transformation is $-2.242 \text{ kJ.mol}^{-1}$ [25], therefore the magnetic contribution of driving force (greater than 0.4 kJ.mol^{-1}) is enough to affect the transformation. As discussed above, the applied magnetic field decreases the transformation velocity in this experiment. This phenomenon was observed in the microstructure, there is more Fe phase left in the sample annealed with HMF (see Fig. 5).

The second factor to affect the transformation velocity is the anisotropic growth of L1_0 FePt, because diffusion along a-axis of L1_0 FePt structure is much faster than along the c-axis [27]. Although L1_0 ordered FePt was paramagnetic at the annealing temperature, the (001) texture in the sample was still enhanced in the direction of the HMF because of high magnetocrystalline anisotropy (observed in the XRD results). The textured FePt separated Fe and Pt. In order for FePt to grow, both Fe and Pt have to diffuse through the FePt phase. The presence of anisotropic interdiffusion in L1_0 FePt leads to anisotropy in growth velocity. In the sample annealed in an out-of-plane HMF, (001) out-of-plane direction was the growth direction of FePt layer. The slower diffusion rate in (001) resulted in low layer growth velocity. In the sample annealed in an in-plane field, (001) texture is enhanced in the direction perpendicular to the FePt layer growth direction. Anisotropic diffusion may have marginal impact on growth of FePt layers.

The third factor to affect the transformation velocity, and the possible reason that cause the stronger transformation inhibition with the in-plane field is the diffusion control. Compared with the samples annealed with an out-of-plane field, the samples with an in-plane field have a much slower transformation velocity (Fig. 5). We attribute this further inhibition of diffusion to the orientation change of the magnetic field to the diffusion control. The effect of HMF on the diffusion of atoms has been investigated in a series of alloys. The effect of magnetic field depends on its orientation, which is applied either perpendicular or parallel to the diffusion orientation. Some research found that the diffusion is inhibited by a perpendicular oriented magnetic field in the alloy of Al-Cu [28], Al-Mn [29], Ni-Al [30]. Youdelis et al. [28] considered that the motion of the diffusion-transported electrons is

inhibited by the Lorentz force in a transverse magnetic field, which in turn requires a corresponding inhibition in ion diffusion to maintain electrical neutrality. The effect of diffusion inhibition by a transverse magnetic field is related to the cyclotron frequency and relaxation time, the mobility of electron and ion, change due to different alloy systems. In some alloy systems, such as Ni-Ti [31], Fe-Ti [32] and Ni-Cu [33] system, however, the effect of a transverse magnetic field on diffusion was found to be negligible. In this experiment of Fe-Pt system, the results show that a diffusion inhibition occurs with the in-plane magnetic field. A detailed discussion of this effect in the Fe-Pt system will be deferred to a later publication.

The magnetic field we have used in this paper are among the highest ever been applied for the annealing process of FePt multilayer or films prepared by any processing method. It is possible that this enhancement of magnetic properties will continue with higher magnetic strength, but further experiments with a new type of magnets are required to determine in the future.

4. Conclusions

We fabricated Fe-Pt magnetic nanocomposite by accumulative roll bonding and annealing under HMF. After six rolling cycles the average thickness of an individual layer was 42 nm. Both TEM and x-ray diffraction data from annealed samples showed the presence of α -Fe, Fe_3Pt , FePt_3 , and Pt phases together with nano-grained L1_0 FePt matrix.

With increasing strength of HMF, the grain size decreased and the internal strain increased. Compared with the annealed Fe-Pt sample without HMF, an out-of-plane field raised the (001) texture of L1_0 FePt phase, and inhibited transformation modestly, whereas an in-plane HMF significantly inhibited the phase transformation.

Magnetic coercivity decreased with increasing annealing temperature and increased with increasing strength of the magnetic field. The remanence and the saturation magnetization increased with increasing magnetic field strength. Sample annealed with a 31.2 T out-of-plane field showed the highest energy product, whereas samples with 31.2 T in plane field showed the lowest energy product. For an in-plane field orientation, the hysteresis loops were not square, and there was an obvious second set of shoulders. The shape of the magnetization curve suggests an inhabitation of transformation by in-plane magnetic field. The inhabitation was attributed to the decreased driving force and increased nucleation barrier caused by the imposed HMF applied in in-plane and out-of-plane directions. The in-plane field has a considerably stronger effect to inhibit the transformation velocity than an out-of-plane field. This was attributed to the diffusion inhibition in Fe-Pt system by a transverse magnetic field.

Acknowledgements

The authors would like to gratefully acknowledge the financial support from the National Natural Science Foundation of China (No. 51674083), the Program of Introducing Talents of Discipline to Universities (the 111 Project of China, No. B07015). The experiments under high magnetic field were undertaken in US National High Magnetic Field Laboratory, which is supported by Florida State and the US NSF (DMR 0654118 and DMR 1157490). We thank Dr. Tyler for editing the manuscript.

References

- [1] C.W. White, S.P. Withrow, K.D. Sorge, A. Meldrum, J.D. Budai, J.R. Thompson, L.A. Boatner, Oriented ferromagnetic Fe-Pt alloy nanoparticles produced in Al₂O₃ by ion-beam synthesis, *J. Appl. Phys.* 93 (2003) 5656–5669.
- [2] J.P. Liu, C.P. Luo, Y. Liu, D.J. Sellmyer, High energy products in rapidly annealed nanoscale Fe/Pt multilayers, *Appl. Phys. Lett.* 72 (1998) 483–483.
- [3] J. Magn. Mater. 262 (3) (2003) 353–360, [https://doi.org/10.1016/S0304-8853\(03\)00062-3](https://doi.org/10.1016/S0304-8853(03)00062-3).
- [4] B.Z. Cui, K. Han, D.S. Li, H. Garmestani, J.P. Liu, N.M. Dempsey, H.J. Schneider-

- Muntau, Magnetic-field-induced crystallographic texture enhancement in cold-deformed FePt nanostructured magnets, *J. Appl. Phys.* 100 (2006) 013902.
- [5] R.F.C. Farrow, D. Weller, R.F. Marks, M.F. Toney, D.J. Smith, M.R. McCartney, Magnetic anisotropy and microstructure in molecular beam epitaxial FePt (110)/MgO (110), *J. Appl. Phys.* 84 (1998) 934–939.
- [6] M.R. Visokay, R. Sinclair, Direct formation of ordered CoPt and FePt compound thin films by sputtering, *Appl. Phys. Lett.* 66 (1995) 1692–1694.
- [7] N.H. Hai, N.M. Dempsey, M. Veron, M. Verdier, D. Givord, An original route for the preparation of hard FePt, *J. Magn. Magn. Mater.* 257 (2003) 139–145.
- [8] D.R. Brown, K. Han, T. Siegrist, T. Besara, R. Niu, High magnetic field annealing of Mn-Ga intermetallic alloys, *MRS Adv.* 1 (2016) 1–7.
- [9] B.Z. Cui, J. Clark, J.W. Sui, K. Han, S.A. Shaheen, Textured anisotropic FePd/ α -Fe nanocomposite foils by sheath repetitive cold-rolling, *J. Alloy. Compd.* 496 (2010) 43–52.
- [10] B.Z. Cui, K. Han, H. Garmestani, H.J. Schneider-Muntau, J.H. Su, J.P. Liu, Enhancement of material properties by magnetic field assisted phase transformation, *Mater. Process. Magn. Fields* (2005) 19–28.
- [11] B.Z. Cui, K. Han, H. Garmestani, J.H. Su, H.J. Schneider-Muntau, J.P. Liu, Enhancement of exchange coupling and hard magnetic properties in nanocomposites by magnetic annealing, *Acta Mater.* 53 (2005) 4155–4161.
- [12] B.Z. Cui, K. Han, Y. Zhang, J.P. Liu, H. Garmestani, S. Liu, H.J. Schneider-Muntau, Crystallization, morphology and magnetic properties of melt-spun (Nd, Pr, Dy)₂(Fe Co, Mo)₁₄B/ α -Fe nanocomposites, *IEEE Trans. Magn.* 40 (2004) 2867–2870.
- [13] K. Han, B.Z. Cui, High magnetic field influences on fabrication of materials with magnetic phases, Feb 25-Mar 01 Orlando, USA, Minerals, Met & Mat Soc, Symposium on Materials Processing under the Influence of External Fields held at the 2007 TMS Annual Meeting, 2007, p. 71.
- [14] P. Jia, J.M. Liu, E.G. Wang, K. Han, The effects of high magnetic field on crystallization of Fe-71(Nb0.8Zr0.2)(6)B-23 bulk metallic glass, *J. Alloy. Compd.* 581 (2013) 373–377.
- [15] P. Jia, E.G. Wang, K. Han, The effects of a high magnetic field on the annealing of (Fe_{0.5}Co_{0.5})(0.75)B_{0.2}Si_{0.05}(96)Nb-4 bulk metallic glass, *Materials* 9 (2016) 899.
- [16] K.Z. Ren, X.H. Tan, H.Y. Li, H. Xu, K. Han, The effects of the addition of Dy, Nb, and Ga on microstructure and magnetic properties of Nd₂Fe₁₄B/ α -Fe nanocomposite permanent magnetic alloys, *Microsc. Microanal.* 23 (2017) 425–430.
- [17] H.Y. Wang, W.H. Mao, W.B. Sun, Y.J. He, S. Mitani, M. Motokawa, High coercivity and small grains of FePt films annealed in high magnetic fields, *J. Phys. D Appl. Phys.* 39 (2006) 1749–1753.
- [18] J.P. Liu, Y. Liu, C.P. Luo, Z.S. Shan, D.J. Sellmyer, Magnetic hardening in FePt nanostructured films, 12-15 Nov. 1996, AIP, USA, 41st Annual Conference on Magnetism and Magnetic Materials, 1997, pp. 5644–5646.
- [19] I. Panagiotopoulos, S. Stavroyiannis, D. Niarchos, J.A. Christodoulides, G.C. Hadjipanayis, Granular CoPt/C films for high-density recording media, *J. Appl. Phys.* 87 (2000) 4358–4361.
- [20] *J. Magn. Magn. Mater.* 198-199 (1999) 486–488, [https://doi.org/10.1016/S0304-8853\(98\)01203-7](https://doi.org/10.1016/S0304-8853(98)01203-7).
- [21] D. Porter, K. Eastering, M. Sherif, *Phase Transformations in Metals and Alloys*, 3rd ed., CRC Press, Boca Raton, 2009.
- [22] T. Garcin, S. Rivoirard, C. Elgoyhen, E. Beaunon, Experimental evidence and thermodynamics analysis of high magnetic field effects on the austenite to ferrite transformation temperature in FeMn alloys, *Acta Mater.* 58 (2010) 2026–2032.
- [23] C.-B. Rong, Y. Li, J.P. Liu, Curie temperatures of annealed FePt nanoparticle systems, *J. Appl. Phys.* 101 (2007) 09K505.
- [24] T. Blubl, D. Goll, Temperature dependence of the magnetic properties of L10-FePt nanostructures and films, *J. Appl. Phys.* 108 (2010) 113910.
- [25] T. Koyama, H. Onodera, Modeling of microstructure changes in FePt nano-granular thin films using the phase-field method, *Mater. Trans. (Japan)* 44 (2003) 1523–1528.
- [26] J. Crangle, G.M. Goodman, The magnetization of pure iron and nickel, *Proc. Royal Soc. London Series A (Math. Phys. Sci.)* 321 (1971) 477–491.
- [27] F. Grostlinger, M. Rennhofer, M. Leitner, E. Partyka-Jankowska, B. Sepiol, B. Laenens, N. Planckaert, A. Vantomme, Anisotropic diffusion in FePt thin films, *Phys. Rev. B (Condens. Matter Mater. Phys.)* 85 (2012) 134302.
- [28] W.V. Youdelis, J.R. Cahoon, Diffusion in a magnetic field, *Can. J. Phys.* 48 (1970) 805–808.
- [29] Z.F. Li, J. Dong, X.Q. Zeng, C. Lu, W.J. Ding, Z.M. Ren, Influence of strong static magnetic field on intermediate phase growth in Mg-Al diffusion couple, *J. Alloy. Compd.* 440 (2007) 132–136.
- [30] R. Xiao, C. Guo-Qing, Z. Wen-Long, W. Cheng-Wei, Z. Jun-Shan, Effect of high magnetic field on intermetallic phase growth in Ni-Al diffusion couples, *J. Alloy. Compd.* 472 (2009) 525–529.
- [31] H. Nakajima, S. Maekawa, Y. Aoki, M. Koiwa, Diffusion of nickel in titanium in a magnetic field, *Trans. Japan Inst. Metals* 26 (1985) 1–6.
- [32] S. Nakamichi, S. Tsurekawa, Y. Morizono, T. Watanabe, M. Nishida, A. Chiba, Diffusion of carbon and titanium in iron in a magnetic field and a magnetic field gradient, *J. Mater. Sci.* 40 (2005) 3191–3198.
- [33] L. Tie, L. Donggang, W. Qiang, W. Kai, X. Zhifeng, H. Jicheng, Enhancement of the Kirkendall effect in Cu-Ni diffusion couples induced by high magnetic fields, *J. Appl. Phys.* 107 (2010) 103542.